Membrane activity detection in cultured cells using phase-sensitive plasmonics

FOOZIEH SOHRABI,[1,2] **YASAMAN JAHANI,**[1] **JOSE VICENTE SANCHEZ-MUT,**[3] **ERSHAD MOHAMMADI,**[1,4] **ZAHRA BARZEGAR,**[5] **XIAOKANG LI,**[1] **LILIANE GLAUSER,**[3] **JOHANNES GRÄFF,**[3] **AND SEYEDEH MEHRI HAMIDI**[2,*]

[1] *Institute of Bioengineering, École Polytechnique Fédérale de Lausanne (EPFL), CH-1015 Lausanne, Switzerland*
[2] *Laser and Plasma Research Institute, Shahid Beheshti University, 1983969411 Tehran, Iran*
[3] *School of Life Sciences, Brain Mind Institute, École Polytechnique Fédérale de Lausanne (EPFL), CH-1015 Lausanne, Switzerland*
[4] *Department of Applied Physics and Institute for Photonic Integration, Eindhoven University of Technology, Eindhoven, Netherlands*
[5] *Department of Statistics, Faculty of Mathematical Sciences, Shahid Beheshti University, 1983969411 Tehran, Iran*
[*] *m_hamidi@sbu.ac.ir*

Abstract: Despite the existence of various neural recording and mapping techniques, there is an open territory for the emergence of novel techniques. The current neural imaging and recording techniques suffer from invasiveness, a time-consuming labeling process, poor spatial/ temporal resolution, and noisy signals. Among others, neuroplasmonics is a label-free and nontoxic recording technique with no issue of photo-bleaching or signal-averaging. We introduced an integrated plasmonic-ellipsometry platform for membrane activity detection with cost-effective and high-quality grating extracted from commercial DVDs. With ellipsometry technique, one can measure both amplitude (intensity) and phase difference of reflected light simultaneously with high signal to noise ratio close to surface plasmon resonances, which leads to the enhancement of sensitivity in plasmonic techniques. We cultured three different types of cells (primary hippocampal neurons, neuroblastoma SH-SY5Y cells, and human embryonic kidney 293 (HEK293) cells) on the grating surface. By introducing KCl solution as a chemical stimulus, we can differentiate the neural activity of distinct cell types and observe the signaling event in a label-free, optical recording platform. This method has potential applications in recording neural signal activity without labeling and stimulation artifacts.

1. Introduction

Understanding the basis of neural activity enables us to perceive the neural networks and their functions. In particular, to determine and identify the activity patterns in the brain provides us with insight to investigate cerebral health and disease. This requires us to study the intercellular signaling activities between individual neurons. So far, researchers have investigated the high-resolution imaging and recording techniques to track neural signals that can be applied at cellular scale [1,2]. However, these techniques suffer from invasiveness (e.g., insertion damages) [3], time-consuming labeling process [4], poor spatial/ temporal resolution [5] and noisy signals [6]. Neuroplasmonic technologies, as a novel branch for neural imaging and signal recording, have excellent potential in satisfying the current challenges due to the label-free, non-toxic and non-photobleaching format, as well as the systemic integration and relatively simple implementation [7,8].

Neuroplasmonic technique probes the biological sample via a light beam and employs the well-known surface plasmon resonance (SPR) sensing mechanism to sensitively reveal minute changes in ion distribution caused by membrane activity [7,9–12]. SPR criterion is based on the resonant oscillation of the free electrons at the metal/dielectric interface which is highly responsive to tiny changes in the dielectric constant on the sensor surface [13]. The physical origin of signal detection using neuroplasmonics is the changes occurred in the dielectric constant of the metal due to the fluctuations in the bilayer formed at the interface where the cell membrane directly contacts the metal surface (i.e., a thin layer of gold). Upon the onset of the neuronal action potential, the redistribution of Na^{2+} and K^+ ions around the bilayer occurs which affects the oscillation activity of free electrons on the metal surface and generates the corresponding SPR signal [14]. By tracking the evolution of the SPR signal, the neuronal signaling event can thus be distinguished without the need of physical electrode probes or external molecular labels [15].

However, the traditional SPR setup suffers from noisy signal since membrane depolarization causes a minor modulation in optical response that is difficult to distinguish from the background noise. Therefore it is critical to improve the technique for increasing the signal to noise ratio (SNR) [16]. Among others, ellipsometry setup is a highly-sensitive measurement technique which records light polarization changes caused by the sample-light interaction in reflection regime [17]. In this technique, a plane electromagnetic wave with p- and s- components is incident on the sample, and the reflected light undergoes both amplitude and phase changes. Here, p and s are the parallel and perpendicular components to the plane of incidence. By denoting the incident electromagnetic waves by E_{ip} and E_{is} and the reflected waves by E_{rp} and E_{rs}, where p and s stand for p- and s-polarizations respectively, we can define the reflection coefficient (R_s, R_p) as $R_s = E_{rs}/E_{is} = \rho_s e^{(i\Delta_s)}$ and $R_p = E_{rp}/E_{ip} = \rho_p e^{(i\Delta_p)}$ where (ρ_s, ρ_p) and (Δ_s, Δ_p) are amplitudes and phase delays for s- and p-waves, respectively. Then we have the complex reflectance ratio, which defines dissimilar reflected electric field amplitudes and the phase delay of one component with respect to the other as $\rho = R_p/R_s = \frac{(E_{rp}/E_{ip})}{(E_{rs}/E_{is})} = \frac{\rho_p e^{i\Delta_p}}{\rho_s e^{i\Delta_s}} = tan\Psi e^{i\Delta}$ where the amplitude attenuation is $\Psi = tan^{-1}\frac{\rho_p}{\rho_s}$ and the phase shift is $\Delta = \Delta_p - \Delta_s$ The main advantage of ellipsometry over SPR measurement is the extra information of the reflected light polarization in addition to the intensity information acquired in SPR measurement. Therefore, by using ellipsometry technique, we can measure both amplitude (intensity) and phase difference of reflected light simultaneously with high resolution and sensitivity [18]. Moreover, this non-destructive method can be used in situ in non-vacuum environments like in liquid while keeping the surface selectivity and sensitivity [19–21]. It provides sufficient temporal resolution in the range of ms to interrogate the dynamics of molecular interaction on the sensor surface [19] and has been applied in various biological studies such as surface concentration variation of biomedical reactions, antigen-antibody binding, hormone-receptor binding and enzymatic reactions on surfaces [19,21,22].

The integration of plasmonic-ellipsometry can provide us the information about detailed optical properties of immobilized biomolecular monolayers, surface concentration variations of biomedical reactions, and kinetic affinity between biomolecules required for further biotech analysis [21]. From a physical viewpoint, the effect of plasmonic resonance in ellipsometric resonance is seen where the amplitude ratio (ψ) reaches its minimum while phase difference undergoes a quick rise near the resonance [23]. The integration of these two powerful methods has greatly augmented the label-free detection resolution [21]. Zhang et al. [24] have detected the neural activity using the shift in the resonance mode of the gold nanoparticle array on indium tin oxide (ITO)-coated glass substrate. In their study, hippocampal neurons were cultured on the gold nanoparticle plasmonic chip and they were chemically stimulated by glutamate injection. In addition, Zhang et al. [25] have successfully detected the neural activity real-time based on localized surface plasmon resonance (LSPR) shift. Ae Kim et al. [26] have recorded simultaneously both optical (i.e. plasmonic) and electrical signals of the nervous tissue under electrical stimulation and they found a good matching except that the optical signals did

not suffer from stimulation artifacts. Poksinski and Arwin [27,28] employed Total Internal Reflection Ellipsometry (TIRE) to study the adsorption of human serum albumin (HSA) and fibrinogen on thin gold films. In particular, by joining the strengths of SPR and ellipsometry, they demonstrated several orders of magnitude increase for the ellipsometry parameters in comparison to conventional ellipsometry setup which was about 72° and 85° increase in Δ parameter for HSA and fibrinogen adsorption, respectively. Furthermore, they showed that the ellipsometry data revealed the information about both protein adsorption and layer reorganization [28]. Later in 2011, Oates et al. [29] have shown that ellipsometry technique not only provided valuable amplitude and phase information but also gave us their relation to plasmonic characteristic of the system.

Previously, we investigated the membrane activity at tissue scale (i.e. cerebellum) for thin-film chips in Kretschmann configuration under electrical stimulation provided by electrode connection [16]. In this study, there is a deeper look at cell scale under chemical stimulation using grating chips. Although top-down fabrication techniques produce high-quality subwavelength grating patterns, they suffer from high cost and time-consuming fabrication procedures [30]. Therefore, we extracted a high-quality grating from the cost-efficient and commercially available Digital Versatile Discs (DVDs) and sputtered thin gold film on it. In this study, we coated the surface of our plasmonic grating with laminin and poly-L-lysine to facilitate cell adhesion and cultured different cells with various levels of membrane depolarization on these gratings. We detected the difference in their cellular signal level in the rest and stimulated states using our constructed optical setup of plasmonic-ellipsometry. This integrated measurement technique provides the capability to observe the intercellular signaling event in an optical, label-free platform. This method has potential applications in recording membrane activity without stimulation and labeling artifacts.

2. Materials and methods

2.1. Fabrication of the plasmonic gratings extracted from commercial DVDs

Typically a DVD consists of multiple layers of a label, a resin layer (polycarbonate), an adhesive layer, a protective layer (hard resin), a reflective layer (e.g., Al), recording layer (pigment material) and the resin layer (polycarbonate). The polycarbonate substrate of a DVD has high-quality patterns applicable as the substrate of our chip. In order to extract polycarbonate grating, DVDs from Verbatim Company with specifications of 16 X, 120 min, 4.7 GB, DVD + R was used. We carefully separated top and down polycarbonate sides of the DVD using a sharp and thin scalpel. Considering the orientation angle φ of the grating as shown in Fig. 1(A), we labeled the desired direction of the grating and we divided the resulted polycarbonate substrate layer was divided into four parts with the size of 25 mm × 30 mm. Then, the gratings were incubated in Ethanol for 5 minutes, rinsed with Ethanol and deionized (DI) water followed by blow drying with N_2. These incubation and washing steps removed the violet-like pigment layer from the surface of polycarbonate grating. Afterward, we uniformly sputtered 30-nm gold on the grating surface with the deposition rate of 13.8 A0.S-1 in the center and 12.3 A0.S-1 in average for 24 seconds using Alliance-Concept DP 650 Sputtering system (Center of Micronanotechnology, EPFL). After coating the gold layer, the chip was ready for cell culture. In Fig. 1(B), it is schematically shown how the neurons were distributed on the grating surface. In our homemade chamber, the grating chip was inserted in one side and on another side, the glass slide was embedded. As shown in Fig. 1(C), the stimulus KCl was injected from the inlet into the medium that filled the inner space of the chamber. K^+ ion elevation due to KCl addition could chemically stimulate the neurons. This subsequently caused the depolarization and ion redistribution at the interface of gold/neurons. The real image of the grating chip in the cell culture medium is shown in Fig. 1(D). The schematic process flow of extracting plasmonic grating is shown in Fig. 1(E) comprising peeling off, pigment removing, blow drying and gold sputtering. In Fig. 1(F), the

topographic image of the polycarbonate grating coated with 30 nm gold is shown. Atomic Force Microscopy images (Bruker FastScan AFM, Center of Micronanotechnology, EPFL) revealed that the structure had an average periodicity of 724 nm and the average height of 162 nm (Fig. S1, Supporting Information).
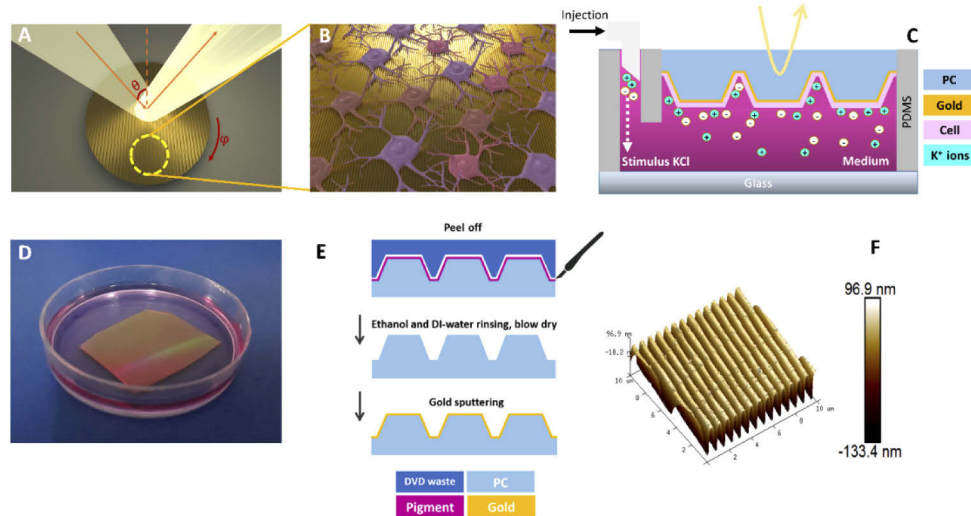
Fig. 1. (A) Schematic of the impinged light on the grating chip with the incident and azimuthal angles denoted by θ and φ. (B) Schematic of the cultured neurons on the chip. (C) Schematic of the chamber with embedded chip and stimulus KCl medium. (D) Real photo of the grating chip with the size of 25 mm × 30 mm in the cell culture medium. (E) Process flow of chip fabrication starting from extracting the grating from a DVD and then depositing gold on it after removing the pigments. (F) AFM image of the grating chip.

2.2. Cell culture

Chips were coated with laminin (33 µg/mL, Invitrogen) and poly-L-lysine to enable cell adhesion [31]. Two cell types of HEK293 embryonic kidney cells (ATCC) and SH-SY5Y neuroblastoma cells (ATCC) were cultured in Dulbecco's modified Eagle's medium (DMEM; Gibco) supplemented with 20% Fetal Bovine Serum (FBS), 100 µ/mL penicillin and 100 mg/mL streptomycin at 37 °C in a humidified atmosphere of 5% CO_2. Primary mouse hippocampal cultures were grown in 35 mm dishes in the media consisting of neurobasal (Invitrogen), B27 supplement (2% w/v), L-glutamine (500 µM) and penicillin/streptomycin (100 U/mL) at 37 °C in a humidified atmosphere of 5% CO_2. All animal procedures were approved by the Service de la consommation et des affaires vétérinaires (SCAV) and carried out according to Switzerland's guidelines on animal welfare (cantonal animal authorisation number VD3169) at the School of Life Sciences (EPFL).

2.2.1. Primary cell culture

For primary hippocampal cell culture, we used the well-known protocol of culturing hippocampal neurons from embryonic rats [32]. Before transferring the cells on the chip, we coated the surface of the chip with Poly-L-lysine in order to satisfy the adhesion condition of the cells to the chip. Falcon 35 mm-petri dishes were used. We coated the chip-containing wells with 1 mL Poly-L-Lysine solution during 2h at room temperature, and subsequently washed them two times with sterile water and dried them under the hood (stored at 4°C maximum 1 week). For fresh medium, we used glucose 30% 10mL consisting of 3 g D-(+)-Glucose Sigma #G5400-250G and

10 mL H_2O. We used Digestion Medium (DM) 10mL/digestion consisting of 9-10 mg L-Cysteine Sigma #C7477-25G, 9.4 mL DM (4°C), 120 µl Glucose 30%, 200U Papain, pH 7.4 adjusted with 5M NaOH, and filtrated 0.22µm filter. DM was preheated at 34°C for 30min (to activate the enzyme) prior to use. For protease inhibitor 10 ml, we used 9.8 mL DM, 120 µl Glucose 30%, and 100 µl Trypsin Inhibitor, filtrated with 0.22 µm filter. The components of 30 ml trituration medium were 26.4 mL MEM #21090022, 360 µl Glucose 30%, 300 µl L-Glutamine 50mM, and 3mL HS (Heat Inactivated -20°C), filtrated with 0.22 µm filter. For 50 ml Neurobasal growth medium, 48 mL Neurobasal, 2 mL B27, 0.5 mL L-Glutamine 50mM, and 0.5 mL Pen/Strep, were mixed and filtrated with 0.22 µm filter. More details of the required materials of the cell culture can be found in the supporting information.

For dissection, the skull was carefully opened and cut to have hippocampus then placed in HBSS medium at room temperature to remove meninges. The tissue was placed in a drop (200ul) of enzyme solution (Digestion medium) and cut with a scalpel into 3 small pieces. The tissue was transferred (using a wide-bore glass pipette) to a 15mL tube containing the digestion medium, and incubated for 30min at 34°C (gently shaking the tube after each 15min). Solution containing tissue was centrifuged 1500 rpm for 1min at RT, tissue-pellet was re-suspended in 10mL Protease Inhibitor, and incubated for 10min at RT. Then, the tube was centrifuged at 1500 rpm for 2min at RT, and tissue-pellet was resuspended in 2 mL of trituration medium. Trituration was performed by pipetting up and down (10-20 times) with 2 mL glass pipette (Corning pyrex7077-2N). After waiting 1-2min to allow large tissue pieces settle down, cell containing supernatant was transferred to a new 15mL tube. The trituration process was repeated until virtually no more large pieces remained (around 9 to 10 times). The new tube was centrifuged 1500 rpm 2-3min at RT, and cell-pellet was resuspended in 10 mL of Neurobasal Growth Medium. Number and cell viability were measured and 2mL, 0.2×10^6 cells/mL per 35mm petri dish containing chip were plated. After 3-4 hours, the Neurobasal Growth Medium was replaced by refreshed 3mL of Neurobasal Growth Medium to remove the dead cells.

2.2.2. Culture of HEK293 and SH-SY5Y cells

The typical protocol for culturing of HEK293 and SH-SY5Y cells from frozen cells in the vials was employed [33]. Cells were stored in the liquid nitrogen and thawed by gentle agitation in a 37°C water bath (approximately 2 minutes). Vial contents were transferred to centrifuge tubes containing 9 mL of 37°C pre-wormed DMEM (Gibco) supplemented with 20% FBS, 100 µ/mL penicillin and 100 mg/mL streptomycin, and span at 125 x g for 5 minutes. Supernatant was removed and cell pellet was resuspended with medium. Cells and viability (Trypan blue) were counted and measured, and 2×10^5 viable cells were seeded in 75 cm^2 flask and incubated at 37 °C in a humidified atmosphere of 5% CO_2 during 3 days for cell recovery. Then, the medium was removed and the cells were briefly rinsed with 0.25% (w/v) Trypsin 0.53 mM EthyleneDiamine Tetraacetic Acid (EDTA) solution, and incubated with 3 mL of Trypsin EDTA solution at 37°C (approximately 5 minutes) to disperse the cell layer. Trypsin digestion was stopped by adding 10 mL of medium, and the cell-containing solution was spun at 125 x g for 5 minutes. Cell pellet was resuspended with 10 mL medium and the cell viability and number were counted again. A total of 2mL 0.2×10^6 viable cells/mL per 35mm petri dish was seeded on the chips.

3. Results and discussion

### 3.1. Chip characterization: preliminary measurements

For recording the control data and their comparison with the main data, chip characterization is necessary. The chip was inserted in our homemade chamber. This chamber had three parts embedded between two metal sheets with central circle openings with the diameter of 10 mm. These three layers were: one ITO-coated square glass slide (703176 Sigma-Aldrich), one

polydimethylsiloxane (PDMS) spacer with the thickness of about 1.7 mm and the grating chip. The ITO-coated glass and the chip were placed in a way that the coated part of the glass and grating faced each other, and the whole layers were clamped. The top part of the chamber was open so we could comfortably inject the solutions into the chamber.

Afterward, we mounted an optical setup by which we could extract the ellipsometric parameters as shown in Fig. S2 in Supporting Information. For mounting the plasmonic-ellipsometry setup, the following parts were set in the following order: broadband Halogen fiber optic illuminator (OSL2, Thorlabs, Inc.) and its collimation package (OSL2COL, Thorlabs, Inc.), iris diaphragm (ID25/M), Glan-Taylor calcite polarizer (GT10-A, Thorlabs, Inc.), optical lens (AC254-035-A1 and LA1805-A, Thorlabs, Inc.), high-precision rotation mount (PR01, Thorlabs, Inc.), 3-Axis NanoMax Flexure Stages (MAX313D, Thorlabs, Inc.), XYZ Translation Stage (PT3/M, Thorlabs, Inc.), optical fiber (QP600-2-VIS-NIR, Ocean Optics, Inc.), spectrometer (Maya200 Pro, the wavelength ranges from 498 nm to 941 nm, the resolution of 0.32 nm, Ocean Optics, Inc.). Using Glan-Taylor calcite polarizer (GT10-A, Thorlabs, Inc.), p and s polarized incident light could be obtained. The spatial resolution of our system according to the spot size of the light onto the sample was 500 μm-1 mm. The temporal resolution of the system has a direct relation with the temporal resolution of the spectrometer. Our spectrometer has the spectral resolution of 0.32 nm and an adjustable integration time between 7.2 ms and 5 seconds. In this study, we focused on broadband analysis; however, the same optical setup can be used for real-time measurement of the neural activity except employing a single-wavelength laser source instead of a broadband Halogen fiber optic illuminator.

First, the chip inside the empty chamber (i.e. air filler) was optically characterized, and for obtaining sufficiently sensitive responses, incident angle θ and azimuthal angle φ were swept experimentally. By fixing incident angle at each step to 40°, 45°, and 50°, the azimuthal angle was swept to 0°, 45°, 90°, 135°, 180°, 225°, 270°, 315° and 360°. The chamber was put in the vertical rotating mount, so φ sweep became possible. In Fig. 2(A), the periodicity direction of the grating with respect to the azimuthal angle was clear. After recording the reflection of the sample under s- and p-polarized incident light and recording these reflections, ellipsometry parameters of Δ and Ψ were extracted using our written FORTRAN code. In Fig. S3 and S4, the experiment and data analysis flowchart were demonstrated, and reflection and ellipsometry graphs for air and water for θ and φ sweep are shown in Fig. S5-20. In these figures, it is shown that θ=40° and φ=90° are optimized angles due to conspicuous resonances so all reported data in this paper are for θ=40° and φ=90°.

For verifying our experimental results, we carried out full-wave simulations using the frequency domain solver of COMSOL Multiphysics 5.3a. Due to the infinite periodicity of the structure in one dimension, we performed the simulations using 2D solver of COMSOL and extremely reduced the running time while increasing the accuracy by fine meshing of the structure. As our grating profile was rather complex, for having a very precise profile of our grating, the geometrical parameters for simulation were extracted from AFM image of the structure as mentioned (Fig. S1) using digitizing which accordingly gave the average height, lattice constant and the thickness of coated gold as 162 nm and 724 nm and 30 nm, respectively. To comply with round corners, which usually arose during the fabrication process, we applied a fillet operator with a radius of 40 nm to the corners vertices. The refractive index for polycarbonate substrate and the gold coating was taken from Ref. [34] where both accounted for the realistic dispersion of materials in the optical regime. After implementing the structure, illumination of a linearly polarized plane wave with θ=40° was performed from the backside of the grating in air background the same as the experiment. Figures 2(B) and 2(C) show correspondingly the reflection spectra in p- and s-polarized illuminations in simulation and experiment where the magnetic and electric fields laid parallel with the infinite periodicity direction (valleys), respectively. In simulation results, it was clear that main resonance happened at 615 nm and 675 nm respectively for p- and s-polarized
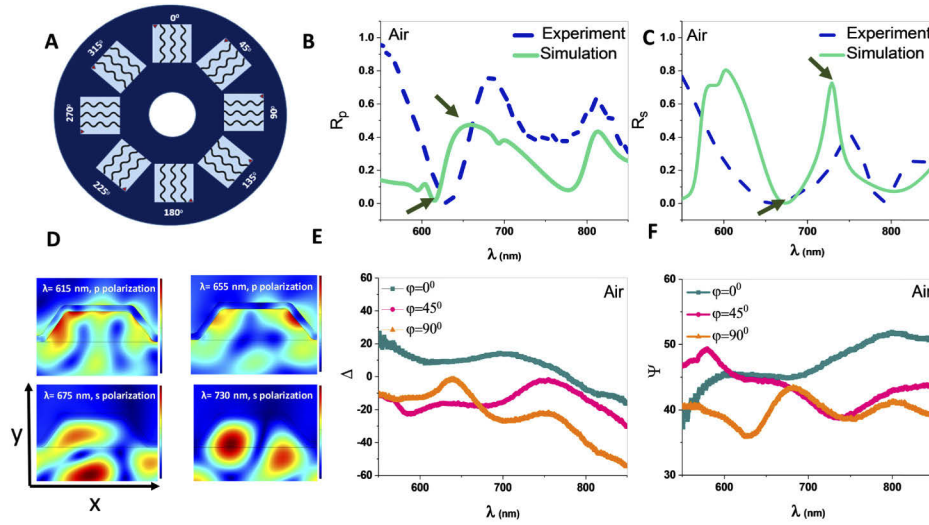
Fig. 2. (A) Grating periodicity direction with respect to the azimuthal angle. Experimental and simulation spectra of the chip in air for θ=40° and φ=90° under p- (B) and s-(C) polarized incident light. (D) Distribution of the total electric field at λ = 615 nm and λ = 655 nm corresponding to the dip and peak resonances in B for p-polarization and λ = 675 nm and λ = 730 nm corresponding to the dip and peak resonances in C for s-polarization. (E) Experimentally extracted ellipsometric parameters of Δ and Ψ from p- and s-polarized reflections for θ=40° and φ = 0°, 45° and 90° where conspicuous resonance is seen for φ = 90° for both Δ and Ψ parameters respectively at 638 nm and 628 nm.

incident light and in experimental results, the main resonance happened at 630 nm and 662 nm respectively for p- and s-polarized incident light. The small difference between simulation and experimental results could be originated from the fabrication since not all parts of the chip might have the exact periodicity of 724 nm and height of 162 nm. In Fig. 2(D), the distribution of the total electric field at the wavelength of 615 nm and 655 nm corresponding to the dip and peak resonances in Fig. 2(B) for p - polarized incident wave and wavelengths of 675 nm and 730 nm corresponding to the dip and peak resonances in Fig. 2(C) for s- polarized incident wave was shown. Experimentally extracted ellipsometric parameters from s- and p-polarized reflections for θ=40° and φ = 0°, 45°, and 90° are shown in Figs. 2(E) and 2(F) where conspicuous resonance is seen for φ = 90° for both Δ and Ψ parameters respectively at 638 nm and 628 nm.

For obtaining the bulk sensitivity of the chip, the same reflection measurement in air case was repeated for deionized (DI) water, glycerol solutions with 60% and 100% weight concentrations (Glycerole Sigma 49767 (≥99.5% (GC)) with refractive indices of 1, 1.333, 1.4134 and 1.4739, respectively. Recorded reflections under s- and p-polarized incident light of θ = 40° and φ = 90° were normalized to s- and p-polarized source spectrum. The normalized reflection under p-polarized incident light for air, water, 60% glycerol and 100% glycerol is shown in Fig. 3(A). By increasing the refractive index of the chamber filler from 1 to 1.4739, the location of the plasmonic resonance was red-shifted from 633.05 nm to 646.79 nm (Fig. 3(B)), leading to a bulk sensitivity (Δλ/Δn) of 60.07 nm/RIU (Fig. S21, Supporting Information).

3.2. Label-free membrane depolarization measurement and analysis

Three cell types of HEK293, SH-SY5Y, and primary hippocampal cells were selected to be cultured on the chips. In order to record the background responses, preliminary measurements were carried out before the cell culture, and the ellipsometric responses of all the chips were
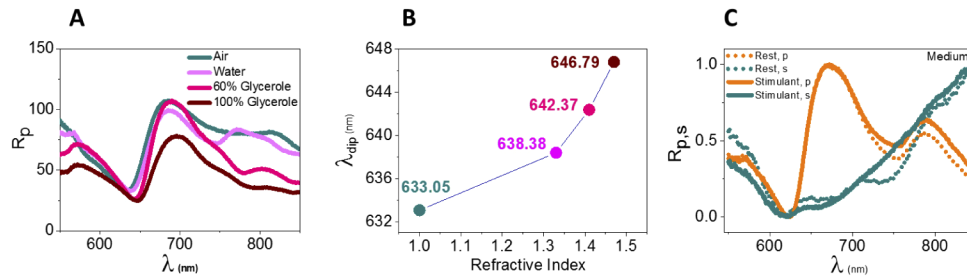
Fig. 3. (A) Reflection in air, DI water, and Glycerol solutions with different concentrations for p-polarized incident light under θ=40° and φ=90° (B) Plasmonic resonance wavelength vs. refractive indices of the solutions mentioned in A. (C) Reflections of the medium in the rest and stimulus states for p- and s-polarized incident light. Spectral positions of plasmonic resonances for both media were roughly the same at 624 nm.

recorded and analyzed for dry (i.e., air) and wet cases (i.e., water, fresh medium, conditioned medium and conditioned medium with KCl stimulus). Conditioned medium (cell secretome) was collected from the cultured cells and it contained the secreted proteins of the cells [35]. The responses of the conditioned medium in contact with the non-cultured chip played the role of background signal. Optical readouts were measured by inserting the chip into individual chambers filled with fresh medium. Afterward, the chambers were unpacked, and chips were rinsed and cleaned. The procedure was repeated for conditioned and stimulus-conditioned medium. Chip reflections with conditioned primary cell medium and stimulus conditioned primary cell medium are shown in Fig. 3(C) with the main plasmonic resonance at 624 m for both media where there is no considerable difference between the optical responses of the rest and stimulus media according to their reflection spectra under p-and s-polarized incident light.

In order to sterilize the polymeric grating structures, the chip was rinsed with ethanol prior to the cell culture. For testing the bacterial contamination, we placed a cleaned chip in a petri dish containing the fresh cell culture medium in the cell incubator and after three days we observed no bacterial contamination. Following the surface functionalization, we seeded three types of cells (i.e., primary mouse hippocampal neurons, HEK293 embryonic kidney cells (ATCC) and SH-SY5Y neuroblastoma cells (ATCC)) on the chip and incubated them. The chip was inserted into the detection chamber filled with non-stimulus medium (rest state), and its reflection spectra were recorded under s- and p- polarized incident light. These reflection data were used to extract Δ and Ψ ellipsometric parameters according to Eq. (1) and 2. For the stimulated state, 50mM KCl solution was loaded into the chamber to chemically stimulate the cell membrane depolarization. As the total volume of the chamber was 440 μL, 22 μL of 1M KCl solution was sampled using a pipette, poured into the chamber and the reflection spectra were re-measured. After KCl addition, there is a time gap of about 1-2 min to perform the measurement and then the optical response was recorded (by pushing the record button, the time-lapse was about 30 seconds to be saved). The final solution had the concentration of 50 mM. Figure 4 shows the reflection spectra and ellipsometry responses of the cultured hippocampal neurons in the rest and stimulated states.

For rest state, the cultured chip responses were normalized to the non-cultured chip ones for the chamber filled with conditioned medium. Similarly, for the stimulated state, the chip responses were normalized to the non-cultured chip ones for the chamber filled with stimulus conditioned medium. In non-cultured chips, the gold surface was in contact with conditioned medium and stimulus medium. As seen in Fig. 3(C), the spectral position of the plasmonic resonances for both media was roughly the same (i.e., 624 nm) since there was not a considerable difference in their refractive indices (about 0.00011). Using Bellingham & Stanley
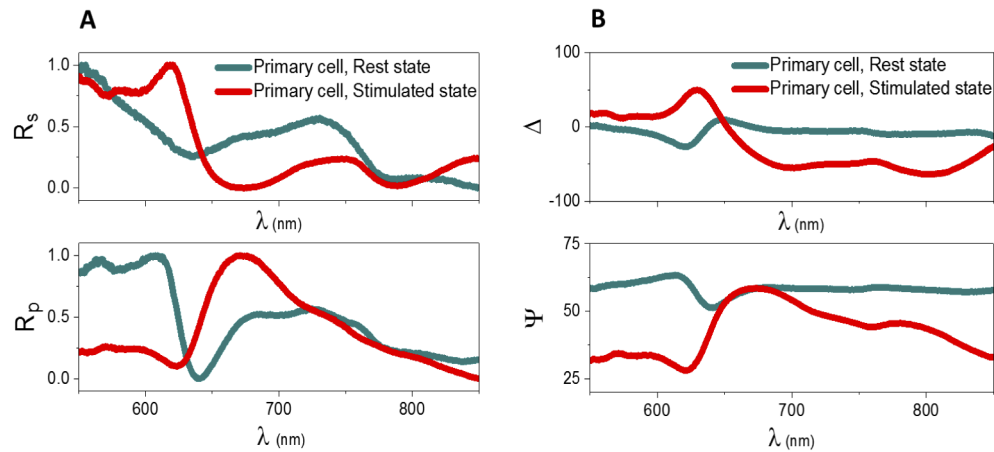
Fig. 4. (A) Reflections of the cultured chip with hippocampal cells in rest and stimulated states for s-and p-polarized incident light. The plasmonic resonances occur for rest and stimulated states at 640 nm and 623 nm, respectively. (B) Extracted Δ and Ψ ellipsometric parameters from A. For the rest state, the resonances in Δ and Ψ occur at 647 nm and 640 nm, respectively. For stimulated state, the resonances in Δ and Ψ occur at 629 nm and 621 nm, respectively. There are the differences of 40.21 and 23.31 for Δ and Ψ values between rest and stimulated states.

RFM342 refractometer, the average refractive indices of the media were measured as following: fresh DMEM ($n_{ave} = 1.33599$), HEK-conditioned DMEM ($n_{ave}=1.33574$), stimulus HEK-conditioned DMEM ($n_{ave} = 1.33585$), SH-SY5Y-conditioned DMEM ($n_{ave} = 1.33568$), stimulus SH-SY5Y-conditioned DMEM ($n_{ave} = 1.33570$), fresh primary cell medium ($n_{ave} = 1.33538$), conditioned primary cell medium ($n_{ave} = 1.33550$) and stimulus conditioned primary cell medium ($n_{ave} = 1.33539$). Therefore, the conditioned primary cell medium and the stimulus-conditioned one had an average refractive index of 1.33550 and 1.33539, respectively. However, for cultured chips, the plasmonic resonance occurred at different positions of 640 nm and 623 nm for rest and stimulated states, respectively. This means that this conspicuous difference in the plasmonic resonance wavelength was originated from the enhanced activity of neurons under chemical stimulation. The reason was that the refractive indices of various filling media had ignorable difference in the order of 10^{-4} which was not detectable according to the bulk sensitivity of our fabricated plasmonic grating. By extracting the ellipsometric parameters from p- and s-polarized reflections of Fig. 4(A) and their depiction in Fig. 4(B), it is observed that not only the resonance wavelength position differed in the rest and stimulus states but also a larger gap was opened between the rest and stimulated states in both Δ and Ψ parameters. Peak resonance wavelengths in Δ are 647 nm and 629 nm and dip resonance wavelengths in Ψ are 640 nm and 621 nm, respectively. The values of Δ are 9.54 and 49.75 for the rest and stimulated states, respectively and for Ψ, this is 51.38 and 28.07 for the rest and stimulated states. Therefore, there was a large difference of 40.21 and 23.31 for Δ and Ψ values between the rest and stimulated states in the gratings with cultured hippocampal cells. We repeated the same procedure for SH-SY5Y and HEK293 cell types. By subtracting the ellipsometric parameters in the rest and stimulated states, we obtained the difference in delta (dΔ) and the difference in Ψ (dΨ) as shown in Figs. 5(A) and 5(B). As shown in Fig. 5(A), for the hippocampal cell the maximum absolute values of dΔ were observed at initial value of i = [626 nm, 71 nm] and final value of f = [700 nm, -49 nm] with the median point at t = [644 nm, 11 nm]. For SH-SY5Y, they were i = [623 nm, 55 nm], f = [645 nm, 33 nm] and t = [633 nm, 44 nm] and for HEK293, they were i = [646 nm, 17 nm], f = [659 nm, 12 nm] and t = [653 nm, 14 nm]. In dΨ graph (Fig. 5(B)), for hippocampal cell they

were i = [618 nm, 34 nm], f = [658 nm, -1 nm] and t = [634 nm, 16 nm], for SH-SY5Y they were i = [614 nm, 25 nm], f = [641 nm, 16 nm] and t = [629 nm, 20 nm] and for HEK293 they were i = [645 nm, 18 nm], f = [656 nm, 17 nm] and t = [650 nm, 17 nm]. So the difference between the rest and stimulated states were as follows: [dλ, dΔ] (hippocampal cell)= [74 nm, -120 nm], [dλ, dΔ] (SH-SY5Y)= [22 nm, -22 nm], [dλ, dΔ] (HEK293)= [13, -5], [dλ, dΨ] (hippocampal cell)= [40, -35], [dλ, dΨ] (SH-SY5Y)= [27, -9] and [dλ, dΨ] (HEK293)= [11, -1]. As seen in Fig. 5, the largest difference in Δ and Ψ was obtained for the chips with hippocampal cell culture.
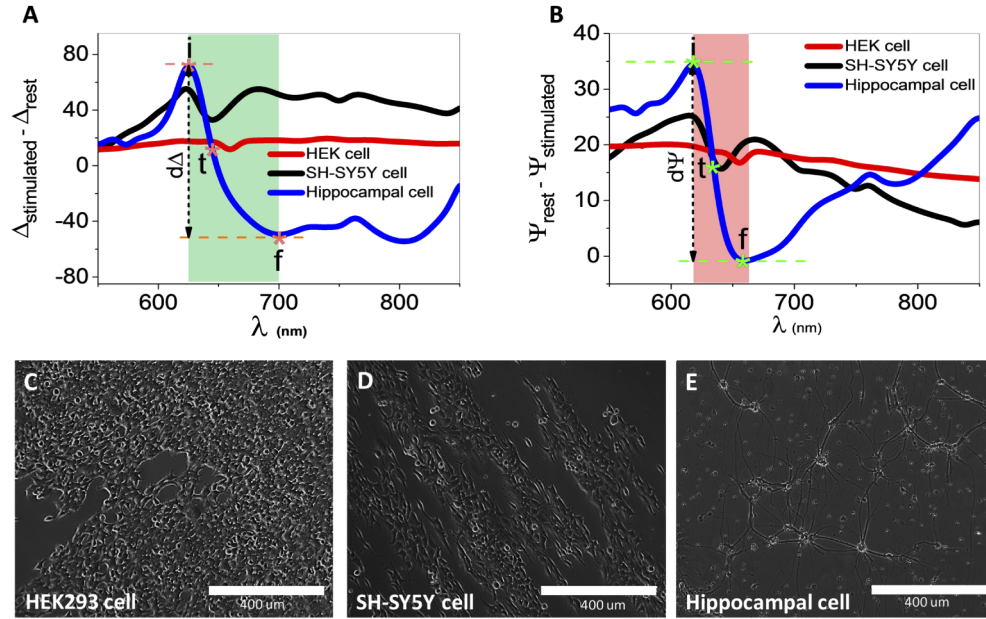
Fig. 5. Difference in ellipsometric parameters of Δ (A) and Ψ (B) for HEK293, SH-SY5Y and hippocampal cells with well-known different levels of electrical activity and voltage-gated channels expression. The largest difference in ellipsometric parameter was observed for hippocampal neurons with high neural activity in highlighted regions. Small difference in ellipsometric parameters was seen for SH-SY5Y and HEK293 cells with lower level of membrane depolarization. Microscopic images of the cultured chips with (C) HEK293 cells (D) SH-SY5Y cells (E) Hippocampal cells.

For both initial (i) and final (f) values in Fig. 5(A), there was a maximum difference between normal (rest) and stimulated states since the absolute value of $|\Delta_{stimulated}-\Delta_{normal}|$ was maximum. Considering Fig. 4(B) and the definition of $\Delta=\theta_p-\theta_s$, for i, this value was positive showing that $|\Delta_{stimulated}|>|\Delta_{normal}|$, $\Delta_{stimulated}>0$, $\Delta_{normal}<0$ so we had the phase retardation for s polarization with respect to p polarization in stimulated case which was vice versa for the rest state. The phase retardation was dominant considering the absolute values of Δ for stimulated and rest states. For final value, $|\Delta_{stimulated}|>|\Delta_{normal}|$, $\Delta_{stimulated}<0$, $\Delta_{normal}<0$ so in both stimulated and rest cases, we had the phase priority in s with respect to p-polarization, however, this phase priority was more significant in the stimulated case. At spectral position of 648 nm, the $\Delta_{stimulated}-\Delta_{normal}$ reached zero meaning that there was no phase retardation difference between rest and stimulated cases. As seen, dΔ was almost the same for the whole spectral range meaning that it did not experience a considerable difference between rest and stimulated states. For Ψ in the rest and stimulated states, the maximum difference between these two cases was observed for i. The graphs of ellipsometry parameters for other incident angles can be found in supporting information (Table S1-S10) besides the dispersion graph in Fig. S22.

As mentioned above, there was not a considerable refractive index change (i.e., 0.00011 in maximum) due to KCl addition to the conditioned medium. The bulk sensitivity of the chip in Fig. 3(B) implied that any considerable changes in the reflected optical signal was not originated by the direct effect of a minute refractive index change. In other words, adding chemical KCl stimulus led to a change in ionic distribution, which consequently affected the plasmons of the interface.

We statistically investigated the significance of the changes in Δ and Ψ parameter in rest and stimulated states. At first step, we used the paired samples t-test for each type of the cultured cells (i.e. hippocampak, SH-SY5Y and HEK293 cells) separately to show that there is a significant difference between for ellipsometry parameters in rest and stimulated states. At the second step, we used one-way analysis of variance (ANOVA) for making comparisons among the three cell types. In this step, we obtained the $\Delta_{contrast}$ ($\Delta_{stimulated}$- Δ_{rest}) and $\Psi_{contrast}$ (Ψ_{rest}- $\Psi_{stimulated}$) and then made the comparison. If a significant difference for the mean values of $\Delta_{contrast}$ and $\Psi_{contrast}$ among three cell types was confirmed, paired comparison test was performed. By making statistical comparison, it was confirmed that the contrast is higher for primary cell type so $\Delta_{contrast}$ (hippocampal)> $\Delta_{contrast}$ (SH-SY5Y)> $\Delta_{contrast}$ (HEK293) and $\Psi_{contrast}$ (hippocampal)> $\Psi_{contrast}$ (SH-SY5Y)> $\Psi_{contrast}$ (HEK293). For carrying out the desired tests, each optical response corresponding to each wavelength was supposed as a repetition. The details of the statistical analysis can be found in the supporting information.

Therefore, the origin of observing these considerable changes in ellipsometry responses in the rest and stimulus media could be investigated in the membrane depolarization of the cells. Cells are surrounded by lipid membranes that are intrinsically impermeable to ions and need transmembrane proteins to be transported through it. Sodium (Na^+) and chloride (Cl^-) ions are more concentrated in the extracellular space, and potassium (K^+) and organic anions (amino acids and proteins) inside of the cells. The family of sodium-potassium pumps actively couple the efflux of three Na^+ ions with the influx of two K^+ ions in an ATP-dependent manner, while the chloride symporter uses the K^+ gradient to couple the efflux of Cl^- and K^+ against Cl^- concentration gradient without the consumption of ATP. These concentration gradients and protein activities create a steady state characterized by a negatively charged intracellular environment relative to the extracellular space, the resting membrane potential, which typically ranges from –40 mV to –80 mV. The opening/closing of ion channels modifies the membrane potential and induces the depolarization, which in the case of the electrically excitable neurons, can be enhanced by the action of voltage-gated channels resulting even in the reversion of the polarity of the membrane potential (from -70mV to +40mV). Considering the selective permeability of the cellular membranes to ions and the negatively charged intracellular environment, the elevation of extracellular K^+ alters the ion gradient reverting the outflow of K^+ and increasing the permeability to Na^+ (voltage-gated channels). This causes the depolarization of the membrane and it has been widely used for studying electrical activity-dependent changes in neurons, muscles, and endocrine cells. In this work, HEK293 cells, neuroblastoma SH-SY5Y cells, and hippocampal neuronal cultures were employed with well-known different levels of electrical activity and voltage-gated channels expression,which directly affects their capacity to respond to KCl-induced depolarization. As shown in microscopic images of the cultured cell on the grating in Figs. 5(C), (D), (E), these cells were successfully cultured on the grating surface. All of these cells can be depolarized, but only the SH-SY5Y and the hippocampal cultures show electrical activity-dependent changes, with a bigger degree the latter where our responses completely satisfied these expectations. Therefore, based on this integrated technique, membrane depolarization level due to chemical stimulation can be distinguished precisely with high spectral resolution.

4. Conclusion

We employed plasmonic-ellipsometry technique to measure the capability to membrane depolarization (electrical activity) of distinct cell types. Regardless of the subtle refractive index difference between conditioned and stimulus medium, the chips presented remarkable changes in their ellipsometric parameters after the elevation of extracellular K^+ due to KCl addition. This means that any considerable changes in the optical signal were not caused by the direct effect of refractive index change of the media but they resulted from the membrane depolarization and ion distribution change, which consequently affected the plasmons of the interface. Different cells with different levels of electrical activity and voltage-gated ion channel expression were chosen. Based on the extracted ellipsometric parameters from our highly-sensitive open optic setup, our expectations could be satisfied that the most significant difference in Δ and Ψ parameters between rest and stimulated states was for the hippocampal cell cultured chip which was expected to have high neural activity. Consequently, intermediate and low optical responses were observed for SH-SY5Y and HEK293 cells with intermediate and low membrane depolarization level. We note that the findings in this study were based on in vitro experiment for the neural activity detection in the cultured cells via integrated plasmonic-ellipsometry technique

Disclosures

The authors declare no conflicts of interest.

See Supplement 1 for supporting content.

References

1. C. J. Goldsmith, C. Städele, and W. Stein, "Optical Imaging of Neuronal Activity and Visualization of Fine Neural Structures in Non-Desheathed Nervous Systems," PLoS One **9**(7), e103459 (2014).
2. E. J. O. Hamel, B. F. Grewe, J. G. Parker, and M. J. Schnitzer, "Cellular level brain imaging in behaving mammals: an engineering approach," Neuron **86**(1), 140–159 (2015).
3. S.-I. Chang, S.-Y. Park, and E. Yoon, "Minimally-Invasive Neural Interface for Distributed Wireless Electrocorticogram Recording Systems," Sensors **18**(1), 263 (2018).
4. T. Kawashima, H. Okuno, and H. Bito, "A new era for functional labeling of neurons: activity-dependent promoters have come of age," Front. Neural Circuits **8**, 37 (2014).
5. B. Burle, L. Spieser, C. Roger, L. Casini, T. Hasbroucq, and F. Vidal, "Spatial and temporal resolutions of EEG: Is it really black and white? A scalp current density view," International Journal of Psychophysiology **97**(3), 210–220 (2015).
6. T. Hasegawa, H. Fujimoto, K. Tashiro, M. Nonomura, A. Tsuchiya, and D. Watanabe, "A wireless neural recording system with a precision motorized microdrive for freely behaving animals," Sci. Rep. **5**(1), 7853 (2015).
7. B. Hyoungwon, J. Sang Beom, J. N. Turner, W. Shain, K. L. Smith, M. L. Shuler, and K. Sung June, "Extracellular Optical Recording Configuration for Neuronal Action Potential Detection by using Surface Plasmon Resonance: Preliminary Experiment," in *Neural Engineering, 2005. Conference Proceedings. 2nd International IEEE EMBS Conference on*, (2005), 332–335.
8. S. Ae Kim, K. Min Byun, J. Lee, J. Hoon Kim, D. G. Albert Kim, H. Baac, M. L. Shuler, and S. June Kim, "Optical measurement of neural activity using surface plasmon resonance," Opt. Lett. **33**(9), 914–916 (2008).
9. H. Raether, *Surface plasmons on smooth and rough surfaces and on gratings* (Springer-Verlag, Berlin, 1986).

10. W. Knoll, "INTERFACES AND THIN FILMS AS SEEN BY BOUND ELECTROMAGNETIC WAVES," Annu. Rev. Phys. Chem. **49**(1), 569–638 (1998).

11. Y. Huang, W. Xie, D. Tang, and C. Du, "Theoretical analysis of voltage-dependent fiber optic surface plasmon resonance sensor," Opt. Commun. **308**, 109–114 (2013).

12. F. Sohrabi, D. Etezadi, R. Perin, Y. Jahani, E. Mohammadi, and S. M. Hamidi, "Phase-sensitive optical neural recording of cerebellum tissue on a flexible interface," J. Appl. Phys. **127**(11), 113101 (2020).

13. S. A. Maier, Plasmonics: Fundamentals and Applications, 1 ed. (Springer US, 2007).

14. S. H. Choi, S. J. Kim, C.-H. Im, S. A. Kim, and D. Kim, "Quantitative model for the change of optical resonance in neural activity detection systems based on surface plasmon resonance," Opt. Laser Technol. **43**(5), 938–948 (2011).

15. F. Sohrabi, S. M. Hamidi, N. Asgari, M. A. Ansari, and R. Gachiloo, "One dimensional photonic crystal as an efficient tool for in-vivo optical sensing of neural activity," Opt. Mater. **96**, 109275 (2019).

16. F. Sohrabi and S. M. Hamidi, "Optical detection of brain activity using plasmonic ellipsometry technique," Sens. Actuators, B **251**, 153–163 (2017).

17. M. Losurdo and K. Hingerl, Ellipsometry at the Nanoscale, 1 ed. (Springer-Verlag Berlin Heidelberg, 2013).

18. T. Oates, H. Wormeester, and H. Arwin, "Characterization of plasmonic effects in thin films and metamaterials using spectroscopic ellipsometry," Prog. Surf. Sci. **86**(11-12), 328–376 (2011).

19. H. Arwin, "Ellipsometry on thin organic layers of biological interest: characterization and applications," Thin Solid Films **377-378**, 48–56 (2000).

20. H. Arwin, M. Poksinski, and K. Johansen, "Enhancement in ellipsometric thin film sensitivity near surface plasmon resonance conditions," Phys. Status Solidi A **205**(4), 817–820 (2008).

21. W.-L. Hsu, S.-S. Lee, and C.-K. Lee, "Ellipsometric surface plasmon resonance," J. Biomed. Opt. **14**, 024036 (2009).

22. H. Arwin, M. Poksinski, and K. Johansen, "Total internal reflection ellipsometry: principles and applications," Appl. Opt. **43**(15), 3028–3036 (2004).

23. R. S. Moirangthem, Y. C. Chang, S. H. Hsu, and P. K. Wei, "Surface plasmon resonance ellipsometry based sensor for studying biomolecular interaction," Biosens. Bioelectron. **25**(12), 2633–2638 (2010).

24. J. Q. Zhang, T. Atay, and A. V. Nurmikko, "Detection of Neural Cell Activity Using Plasmonic Gold Nanoparticles," in *Conference on Lasers and Electro-Optics/Quantum Electronics and Laser Science Conference and Photonic Applications Systems Technologies, OSA Technical Digest (CD)* (Optical Society of America, 2008), CWM3.

25. J. Zhang, T. Atay, and A. V. Nurmikko, "Optical Detection of Brain Cell Activity Using Plasmonic Gold Nanoparticles," Nano Lett. **9**(2), 519–524 (2009).

26. S. Ae Kim, K. Min Byun, J. Lee, J. Hoon Kim, D.-G. Albert Kim, H. Baac, M. L. Shuler, and S. June Kim, "Optical measurement of neural activity using surface plasmon resonance," Opt. Lett. **33**(9), 914–916 (2008).

27. M. Poksinski and H. Arwin, "Protein monolayers monitored by internal reflection ellipsometry," Thin Solid Films **455-456**(721), 716–721 (2004).

28. M. Poksinski and H. Arwin, "Total internal reflection ellipsometry: ultrahigh sensitivity for protein adsorption on metal surfaces," Opt. Lett. **32**(10), 1308–1310 (2007).

29. T. W. H. Oates, H. Wormeester, and H. Arwin, "Characterization of plasmonic effects in thin films and metamaterials using spectroscopic ellipsometry," Prog. Surf. Sci. **86**(11-12), 328–376 (2011).

30. F. Sohrabi and S. M. Hamidi, "Fabrication methods of plasmonic and magnetoplasmonic crystals: a review," Eur. Phys. J. Plus **132**(1), 15 (2017).

31. Protocols, retrieved December 2019, https://www.protocolsonline.com/recipes/stock-solutions/polylysine-coated-tissue-culture-surfaces/.

32. S. Kaech and G. Banker, "Culturing hippocampal neurons," Nat. Protoc. **1**(5), 2406–2415 (2006).

33. A. T. C. C. (ATCC), (American Type Culture Collection (ATCC) 2019), retrieved https://www.atcc.org › CRL-1573.

34. M. N. Polyanskiy, "Refractive index database" (2018), retrieved https://refractiveindex.info.

35. P. Dowling and M. Clynes, "Conditioned media from cell lines: a complementary model to clinical specimens for the discovery of disease-specific biomarkers," Proteomics **11**(4), 794–804 (2011).